Earth and Planetary Science Letters 373 (2013) 1–7

Contents lists available at SciVerse ScienceDirect

Earth and Planetary Science Letters

journal homepage: www.elsevier.com/locate/epsl

Statistical properties of low-frequency earthquakes triggered by large earthquakes in southern Taiwan

Chi-Chia Tang [a,*], Zhigang Peng [b,1], Cheng-Horng Lin [a,2], Kevin Chao [b,c,3], Chau-Huei Chen [d,4]

[a] Institute of Earth Sciences, Academia Sinica, 128, Section 2, Academia Road, Nangang, Taipei 11529, Taiwan
[b] School of Earth and Atmospheric Sciences, Georgia Institute of Technology, 311 Ferst Drive, Atlanta, GA 30332, USA
[c] Earthquake Research Institute, University of Tokyo, 1-1-1 Yayoi, Bunkyo-ku, Tokyo 113-0032, Japan
[d] Department of Earth and Environmental Science, National Chung Cheng University, 168 University Road, Min-Hsiung, Chia-Yi County 62102, Taiwan

ARTICLE INFO

Article history:
Received 5 September 2012
Received in revised form
20 April 2013
Accepted 21 April 2013
Editor: P. Shearer

Keywords:
Taiwan
low-frequency earthquake
triggered tremor
non-volcanic tremor

ABSTRACT

The recent discovery of triggered tremors (TTs) and low-frequency earthquakes (LFEs) in various tectonic environments provides an opportunity for studying the fundamental properties and physical mechanisms of deep tectonic tremor. Here, we quantify the relationship between TTs and LFEs beneath the Central Range in southern Taiwan and their statistical properties during the teleseismic waves of six large distant earthquakes. Using waveforms of 11 LFEs triggered by the 2005 M_w 8.6 Nias earthquake as templates, we scan through 12 hours of waveform data around six mainshocks and identify a total of 783 LFEs. The LFEs were mainly located in a compact region between 12 and 36 km in depth near the Chaochou–Lishan Fault. Most of LFEs occurred within TT during the passage of large-amplitude surface waves, and the increase of the LFE rate during the surface waves is statistically significant. The LFE rates do not follow an Omori's type decay, but rather abruptly return to the background rate immediately after the surface-wave passage. These findings suggest that LFEs do not trigger any additional LFEs at later times and are primarily driven by an external forcing. Our observations are consistent with the inference that TTs consist of many reoccurring LFEs.

1. Introduction

Tremor away from volcanoes (Obara, 2002) and triggered by seismic waves, termed triggered 'non-volcanic' or 'deep tectonic' tremor (TT), reflects shear slip on deep active faults driven by transient dynamic stresses (Peng and Gomberg, 2010, and references therein). Relative to regular earthquakes, TTs have been exclusively observed near major plate boundaries: California (Ghosh et al., 2009; Peng et al., 2009, 2010), Japan (Miyazawa and Brodsky, 2008; Chao et al., 2013), New Zealand (Fry et al., 2011), Vancouver Island (Rubinstein et al., 2007, 2009), Haida Gwaii (or Queen Charlotte) Island (Aiken et al., 2013), Cuba (Peng et al., 2013) and Taiwan (Tang et al., 2010; Chao et al., 2012). It is well known that the durations of triggered and ambient tremors are longer than ordinary earthquakes, and they are dominated by low-frequency seismic energy of 1–10 Hz, as compared with regular earthquakes (Nadeau and Dolenc, 2005; Peng et al., 2008).

Low-frequency earthquake (LFE), a new class of seismic event, was first identified by the Japan Meteorological Agency (JMA) in their seismicity catalog in southwest Japan (Katsumata and Kamaya, 2003). Shelly et al. (2006) hypothesized that the reduction of effective stress due to elevated pore-fluid pressure might help promote LFE and tremor generation, and tremors could be considered as a swarm of many LFEs (Shelly et al., 2007). Recent studies of repeating LFEs families along the Parkfield–Cholame section of the San Andreas Fault also confirmed that TTs can be largely explained by the same LFE families that occurred during ambient tremor episodes (Shelly et al., 2011). Tang et al. (2010) identified LFEs within TTs beneath the southern Central Range of Taiwan and further confirmed that TTs consist of many LFEs. The hypocentral depths of these LFEs range from 12 km to 38 km and the epicenters are near the Chaochou–Lishan Fault (CLF), a major reverse fault in Taiwan. Local seismic tomography (Wu et al., 2007) reveals a relatively high ratio of P-to-S wave velocity (V_p/V_s ratio) area near the hypocenter of LFEs, suggesting the existence of pore fluids.

The primary objective in this study is to further investigate the statistical properties of LFEs in Taiwan around several large teleseismic mainshocks and their relationship with TTs observed in recent studies (Chao et al., 2012, 2013). *Note that in this paper*

* Corresponding author. Tel.: +886 5 2783 9910x523; fax: +886 2 2783 9871.
E-mail addresses: iori897@gmail.com (C.-C. Tang), zpeng@gatech.edu (Z. Peng), lin@earth.sinica.edu.tw (C.-H. Lin), kchao@eri.u-tokyo.ac.jp (K. Chao), seichen@eq.ccu.edu.tw (C.-H. Chen).
[1] Tel.: +1 404 894 0231; fax: +1 404 894 5638.
[2] Tel.: +886 2 2783 9910x521; fax: +886 2 2783 9871.
[3] Tel.: +81 804 447 3228.
[4] Tel.: +886 5 2720 411x66202; fax: +886 5 2720 807.

0012-821X/$ - see front matter © 2013 Elsevier B.V. All rights reserved.
http://dx.doi.org/10.1016/j.epsl.2013.04.039

we do not attempt to resolve the issue as to whether LFEs are fundamentally different from TT, or simply higher amplitude or more resolvable parts of TT. Our observations, as will be shown below, are consistent with TT being composed of multiple LFEs. But for convenience, we will continue to use the term LFE for the repeatable waveforms that we identify with a matched-filter scanning approach.

We focus on the southern Central Range in Taiwan, mainly because tremors in this region have been repeatedly triggered by the surface waves of recent large teleseismic earthquakes (Peng and Chao, 2008; Tang et al., 2010; Chao et al., 2012). The conventional technique for locating tremor often uses differential S-wave arrival times from tremor envelopes (Obara, 2002; Chao et al., 2012), which have the difficulty of obtaining accurate tremor location, especially the depth. Identifying P- and S-waves of LFEs within tremors provides another way to accurately locate tremor sources (e.g., Shelly and Hardebeck, 2010). However, direct investigation of LFEs is difficult due to low amplitudes and overlapping P-wave arrivals. Hence, we use waveforms of LFEs triggered by the 2005 Nias M_w 8.6 earthquake (Tang et al., 2010) as templates to scan through several hours of data before and after triggering mainshocks. In the following section, we first describe briefly our LFE scanning technique and how we quantify the repeating LFEs families among different triggering events. Then we analyze their statistical properties and discuss the connection between the detected LFEs and TTs.

2. Data and analysis processes

We focused on six large teleseismic earthquakes (Table S1) that have triggered tremors in southern Taiwan (Chao et al., 2012). Their sources are close to centroid of LFEs triggered by the 2005 Nias earthquake (Tang et al., 2010). We utilized the waveform data recorded by the Broadband Array in Taiwan for Seismology (BATS), operated by the Institute of Earth Sciences, Academia Sinica and the Central Weather Bureau, and by the Central Weather Bureau Seismic Network (CWBSN) (Fig. 1). The BATS stations are equipped with broadband sensors (Trillium) and digital recorders (Q330), while the CWBSN stations have 1 Hz S13 short-period sensors (Teledyne Geotech).

The analysis process generally follows that of Tang et al. (2010) and is described here. We analyzed the waveform data 6 h before and after the origin time of the six mainshocks. The selected time period not only includes the large-amplitude teleseismic waves, but also spans a long-enough time period to provide an estimation of the background LFE rate. Because sampling rates of the stations of the BATS (20 sample s^{-1}) and the CWBSN (100 sample s^{-1}) are different, we first cut different time segments of data for each earthquake according to the duration of surface waves, apply a 2–8 Hz band-pass filter to remove long-period surface waves and then re-sample to 20 sample s^{-1}. We basically focused on TT signals within 2–8 Hz band-passed-filtered waveforms according to previous studies (Chao et al., 2012, 2013).

Next we used the same 11 LFEs templates triggered by the 2005 M_w 8.6 Nias earthquake (Tang et al., 2010) as templates to scan through the 12-h waveform for all six mainshocks. This is the so-called matched filter technique (Gibbons and Ringdal, 2006) that has been widely used to detect LFEs within tremor (Shelly et al., 2007; Brown et al., 2008, 2009; Tang et al., 2010) and missing early aftershocks following large earthquakes (Peng and Zhao, 2009). In detail, we first cut 3 s before and after the S-wave arrivals of each template. We then calculated the correlation coefficient (CC) values for the three-component seismograms among all stations for each time window that steps forward at 0.05 s (1 sample). We also computed a network averaged CC value for all time windows. Lastly, we applied a threshold based on five times the median absolute deviation (MAD) of each CC values to detect candidate events.

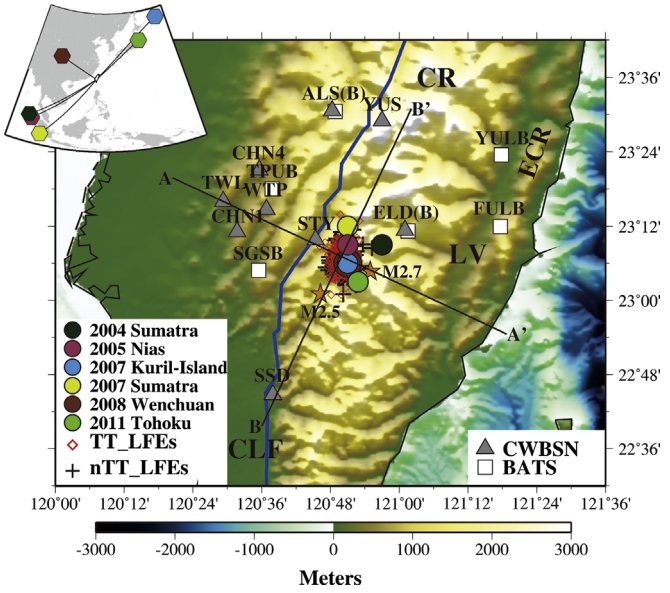

Fig. 1. Epicenters of low-frequency earthquakes (LFEs) within tremors triggered by large teleseismic events. The solid circles with different colors represent the location of triggered tremors reported by Chao et al. (2012). The open red diamonds and crosses correspond to location of LFEs within (TT_LFEs) and out of triggered tremors (TTs) segments (nTT_LFEs), respectively. Two orange stars represent local earthquakes occurred during the 2004 M_w 9.0 Sumatra earthquake and their origin times are marked in Fig. 3. The blue line represents the strike of Chaochou–Lishan fault (CLF). Profiles AA′ and BB′ are perpendicular and parallel to the Central Range (CR), respectively, and the cross-section plots are shown in Fig. 5. Seismic stations of BATS and CWBSN are denoted by white squares and gray triangles, respectively. The inset shows the epicentral locations (hexagons) and the ray paths of the six triggering mainshocks. LV: the Longitudinal Valley. ECR: Eastern Costal Range. (For interpretation of the references to color in this figure legend, the reader is referred to the web version of this article.)

After detecting candidate events, we added 2 s (1 s before and after the original 6-s window) to the waveforms of the newly detected events. We decreased the time window of the template waveforms to 4 s and scanned the template through the 8-s time segment to detect S-wave arrivals on the horizontal components. To identify as many LFEs as possible without sacrificing the robustness of the results, we set a threshold of 12 times the MAD for waveform detection. The same procedure was applied to search for P-wave arrivals in vertical component. Fig. 2 shows an example of detected P and S waves of a LFE for the 2004 M_w 9.0 Sumatra earthquake. More examples are shown in Fig. S1.

Once we obtained the P- and S-wave arrivals of the newly detected events, we determined the differential travel times of the P- and S-waves based on waveform cross-correlations from the 4-s window. We then used hypoDD double-difference algorithm (Waldhauser and Ellsworth, 2000) with a 1-D velocity model under southern Taiwan (Tang et al., 2010) to locate the detected LFEs. We required at least three stations with both P- and S-wave arrivals and eight link pairs of the P or S wave in locating LFEs.

To examine the statistical significance of detected LFEs during large-amplitude surface waves, we computed a β-statistic value (Aron and Hardebeck, 2009), which is a measure of the difference between the observed number of events after the mainshock and the expected number from the background rate before the mainshock. We use the 6-h window before the mainshock to compute the background LFE rate. The time window after the mainshock starts from the predicted P-wave arrival and stops at the end of TT period as reported by previous studies (Chao et al., 2012, 2013). The β-value is defined as follows:

$$\beta = \frac{\mathrm{Na} - N\mathrm{Ta}/T}{\sqrt{N(\mathrm{Ta}/T)(1-\mathrm{Ta}/T)}} \quad (1)$$

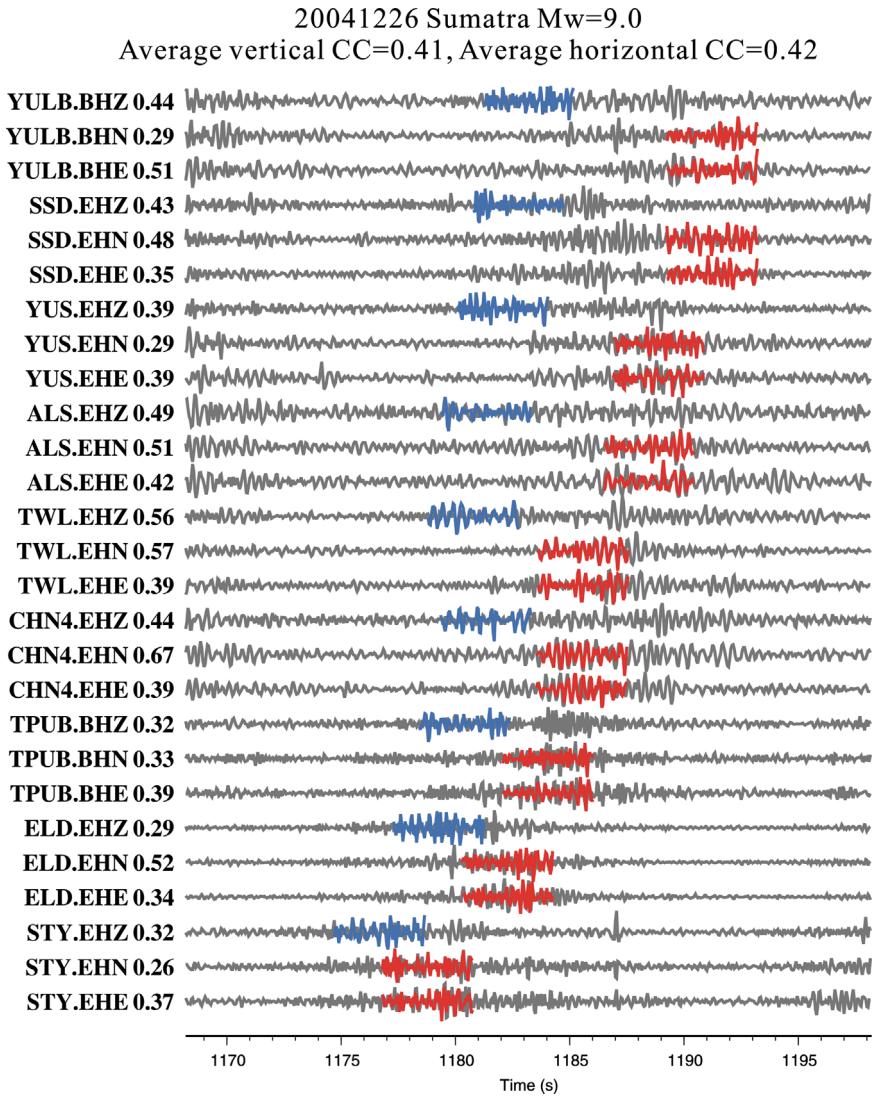

Fig. 2. Waveform detections of a low-frequency earthquake (LFE) during the teleseismic waveforms of the 2004 M_w 9.0 Sumatra earthquake. The gray lines show the continuous waveforms, and the blue and red lines show the P and S waves of a template event. All seismograms were band-pass-filtered at 2–8 Hz and times were relative to the original occurrence time of the Sumatra mainshock. The station/channel names and the correlation coefficients are marked on the left. (For interpretation of the references to color in this figure legend, the reader is referred to the web version of this article.)

where Na and N are the number of events in the interested period and total number of events, respectively. Ta and T are the time length of interest and the whole time period, respectively. For absolute values of $\beta \geq 1.64$, the difference in seismicity rate between the two time periods is significant at 90% confidence level, and for $\beta \geq 2.57$, it is significant at 99% confidence level (Aron and Hardebeck, 2009).

3. Results

We detected a total of 783 LFEs during the 12-h period for six mainshocks (Table S1). Fig. 3 shows temporal behaviors of LFEs 6 h before and after the 2004 M_w 9.0 Sumatra earthquake. A total of 111 LFEs were detected in this case (Fig. 3a). Among them, 60 occurred during the TT period (Fig. 3b). The β-value is 38.65, suggesting that the triggering of LFEs is statistically significant. The cumulative LFEs show a rapid increase in seismicity rate of LFEs after the Love-wave arrival, followed by a gradual decay during the subsequent Rayleigh waves between 1400 and 1800 s (Fig. 3b). The LFE rate during the TT period (e.g. between 900 and 1600 s) is roughly nine times ($\sim 0.09\ s^{-1}$) of the time segment before the Love wave ($\sim 0.01\ s^{-1}$). This time period coincides with the observed triggered tremor between 900 and 1600 s after the mainshock (Chao et al., 2012). The LFE rate of $0.01\ s^{-1}$ (Fig. 3) likely corresponds to the background rate in this region. The tremor-like signals at STY before the P wave were only found at this station, and hence they are likely local noise signals rather than deep tremor. Most of the LFEs occurred in the depth range of 15 and 27 km (Fig. 3c) and were detected within the TTs (Fig. 3d).

The detection for the 2005 M_w 8.6 Nias earthquake shows slightly different results (Fig. S2). We obtained 150 detections and 72 of them were detected during the TT period (Fig. S2a and b). The LFE numbers slowly increase between the P- and Love-wave arrivals and the LFE rate during this period is $\sim 0.03\ s^{-1}$ (Fig. S2b), which is higher than that of the 2004 Sumatra event. This is lower than the LFE rate of $\sim 0.07\ s^{-1}$ during the TT period. The LFEs mainly concentrated between 12 and 30 km at depth and the β-value is 36.69 (Fig. S2c and d). Similar LFE occurrence can be observed in the 2007 M_w 8.1 Kuril-Island (Fig. S3) and the 2007 M_w 8.4 Sumatra earthquake (Fig. S4). The cumulative LFEs show a rapid increase in seismicity rate of LFEs, followed by a slow decay similar to the 2004 Sumatra event. The β-values are 25.37 and 26.43.

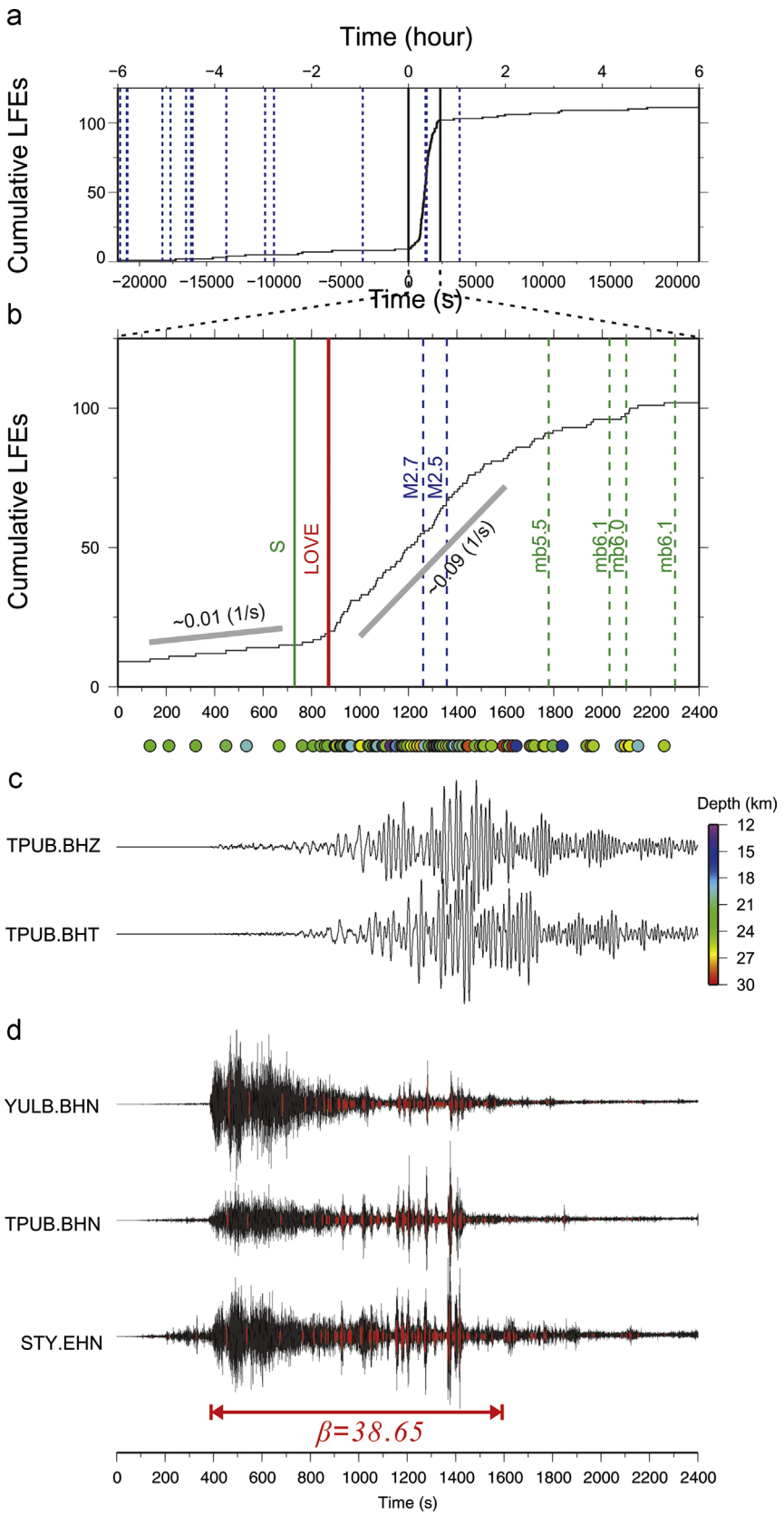

Fig. 3. Low-frequency earthquakes (LFEs) triggered by the 2004 M_w 9.0 Sumatra earthquake. (a) Cumulative number (black line) of detected LFEs during a 12-h period centered on the origin time of the mainshock. The blue dashed lines indicate origin times of local earthquakes. (b) A zoom-in plot of the cumulative number of LFEs around the mainshock. The LFE rates before Love-wave arrival and during triggered tremor (TT) period are ~0.01 and ~0.091 s^{-1}, respectively. The dashed green lines mark the theoretical S-wave arrivals of aftershocks with $m_b \geq 5.5$. The dashed blue lines mark the origin times of two local earthquakes from the CWB catalog. (c) Detected LFEs (color-coded by their depth) during 0 and 2400 s beginning from the origin time of mainshock. (d) Waveforms after applying 2–8 Hz band-pass filter for north–south components at different stations. The red lines mark the waveforms of the detected events. The β-value is 38.65. (For interpretation of the references to color in this figure legend, the reader is referred to the web version of this article.)

The 2008 M_w 7.9 Wenchuan earthquake triggered widespread tremors in southwest Japan (Miyazawa et al., 2008), Cascadia (Gomberg, 2010), and central California (Peng et al., 2009). However, the tremor signals in Taiwan triggered by this main shock were barely observed between 600 and 850 s during the large-amplitude surface waves, likely because of the high pre-event noise and long-lasting P- and S-wave coda (Chao et al., 2012). This could be the same explanation for why we detected a relative low number of LFEs (10 out of 52 detections) during the TT period (Fig. S5). The 2011 M_w 9.0 Tohoku earthquake also triggered widespread tremors around the world (Chao et al., 2013; Gonzalez-Huizar et al., 2012) and were followed by several early aftershocks with $M \geq 6.0$. Here we identified 131 LFEs in the 12-h window (Fig. S6). The cumulative curve of LFEs again shows clear increase in the number of LFEs after the arrivals of long-period Love wave (Fig. S6b). The teleseismic P waves of some large aftershocks may have obscured some LFE detections. However, the β-value is 21.22, again suggesting a statistically significant increase in the LFE rates.

To examine whether the rate of LFEs decays following an Omori-like pattern, we shifted the occurrence time of LFEs according to their predicted Love-wave arrivals (with an apparent velocity of 4.1 km/s) (Chao et al., 2012) and stacked the LFEs of 12-hour windows for the six mainshocks (e.g., Velasco et al., 2008). Fig. 4 shows the stacked rate for every 15 min relatively to the Love-wave arrivals. The LFE rate a few hundred seconds after Love-wave arrival is at least 30 times higher than those outside surface waves (Fig. 4a). The LFE rate returns to the pre-mainshock level immediately afterward.

To compute more detailed changes in LFE rate, we use a window of five data point and slide forward one data point per time, plotting the resulting LFE rate in a log–log scale (e.g., Ziv et al., 2003; Peng et al., 2007). Fig. 4b shows that the LFE rates before and after the teleseismic waves are similar. The rate increases significantly around ~500 s before the Love waves, likely reflecting possible triggering by the teleseismic P and S waves. The LFE rate is the highest during the ~1000 s after the predicted Love wave arrivals. Then the rate drops abruptly to the background level within the next ~1000 s or so.

The LFEs were mainly located near the CLF beneath the southern part of the Central Range and their hypocenters distributed from 12 to 36 km at depth (Fig. 5). The epicenters of LFEs detected in this study and TTs reported by Chao et al. (2012, 2013) are shown in Fig. 1. TTs are located in the same vicinity as LFEs, i.e. near the CLF, except for the tremors triggered by the 2004 Sumatra event. To further investigate the spatial distributions of LFEs, we classified LFEs into two groups according to their occurrence within or outside of TT time periods. Both groups occurred in similar regions (Figs. 1 and 5), suggesting that they originate from similar source processes.

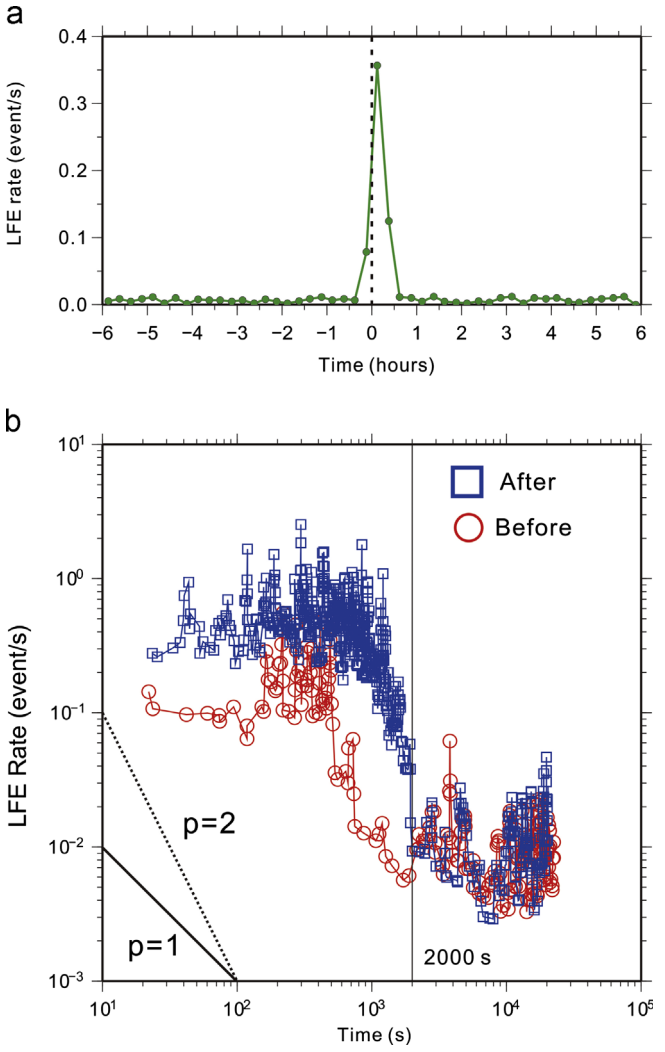

Fig. 4. Stacked low-frequency earthquake (LFE) rate before and after the triggering mainshock. (a) The LFE rate within 6 h before/after the Love-wave arrivals. The rate is computed every 15 min. (b) The LFE rate in a log–log plot before (red circles) and after (blue squares) the Love wave arrivals. The solid and dotted lines show the reference rates with $p=1$ and 2. The vertical dashed line marks the approximate time of 2000 s when the LFE rate returned to the pre-mainshock level. (For interpretation of the references to color in this figure legend, the reader is referred to the web version of this article.)

4. Discussions

In this study we analyzed waveform data 6 h before and after six mainshocks to detect LFEs in southern Taiwan. Because LFEs usually have low signal-to-noise ratios, correlations from individual seismograms cannot be used to detect new LFE events. Here we simultaneously considered waveforms across the network, which provides more reliable detection power. In addition, a benefit of using previously identified LFEs as templates is that we could detect LFEs which reoccurred in similar regions over time.

Owing to the high-density seismic networks, we detected a total of 783 LFEs within the 12-hour time windows. Among them, 280 LFEs occurred during the tremor episodes triggered by the six teleseismic earthquakes. In all cases, the LFE rates show statistically significant increases during the large-amplitude surface waves, suggesting that dynamic stresses from large-amplitude surface waves triggered the LFEs. In addition, the LFEs and the TTs were located by different techniques, but they occurred in similar regions. The observations further confirmed that TT signals could be explained by many overlapping LFEs (Tang et al., 2010; Shelly et al., 2011). LFEs detected within and outside of TT periods share similar regions (Figs. 1 and 5), indicating that tremors occurring outside the surface wave windows also consist of similar sets of LFEs (Shelly et al., 2007).

One interesting observation is that the LFE rates drop abruptly after the passage of the teleseismic surface waves (Fig. 5b). If we manage to fit a power-law curve, the resulting Omori-law p value is about 2, which is much higher than the typical p value of 1 (Brodsky, 2006) for dynamically triggered microearthquakes in geothermal regions. Brodsky (2006) found that prolonged sequences of remotely triggered earthquakes follow an Omori-law decay of 1, similar to regular aftershock sequences (Utsu et al., 1995). They suggested that the instantaneously triggered earthquakes could trigger additional earthquakes at a later time, and the mechanisms of near-field aftershocks and long-range triggered earthquakes could be similar. Here, the LFEs

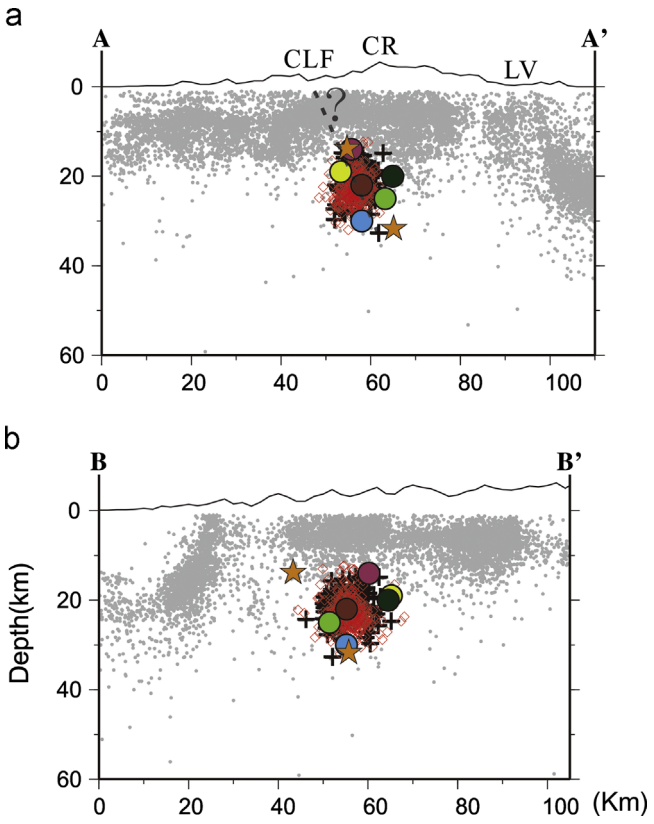

Fig. 5. Hypocentral locations of all low-frequency earthquakes (LFEs) and the six triggered tremors (TTs) along the AA′ (a) and the BB′ (b) profiles. The gray dots indicate the background seismicity from 1991 to 2008 listed in the CWB catalog. The depth distributions of LFEs are from ~12 to 36 km which are below the local earthquakes. Other symbols and notations are the same as in Fig. 1.

abruptly ended shortly after the surface waves, without showing any prolonged activity like aftershocks or triggered earthquakes. This observation is similar to the abrupt cessation of triggered tremors at Parkfield following the 2004 Sumatra earthquake (Ghosh et al., 2009) and at Taiwan following the 2011 Tohoku earthquake (Chao et al., 2013), suggesting that LFEs require a driving force from external forcing. The external forcing could be dynamic stresses from large-amplitude teleseismic waves (e.g., Peng and Gomberg, 2010), tidal stresses (Rubinstein et al., 2008; Thomas et al., 2009), and/or spontaneous creep by nearby slow-slip events (Shelly, 2010).

One may argue that mixing signals from early aftershocks could cause the abrupt cessation of the LFE rate. While some large teleseismic aftershocks could obscure the detection of LFEs during the time period we analyzed (e.g., Fig. S6), we did not see a clear change in the LFE rates for most early aftershocks with $m_b > 5.5$ in other cases (Figs. 3, S2–S6). In addition, because the aftershock rates also decay with time, LFEs occurring at later times were less obscured by teleseismic aftershocks. Finally, as shown in Fig. 5b, the LFE rates long before and after the teleseismic waves were very similar, again suggesting that large early aftershocks did not obscure most of LFE detections during the time period we analyzed.

In this study, we detected LFEs before P-wave arrivals of different mainshocks. In several cases, LFEs were detected during the teleseismic P waves of the mainshock (e.g., Fig. 3), aftershocks (Fig. S6), or local earthquakes (Figs. 3, S2 and S3), which raised the suspicion of false detections due to random combinations of high-frequency signals. Several lines of evidence suggest that most of our detections are valid. First, we use a rather high threshold of 12 times the MAD to detect LFEs. For a normal distribution of random variables, the corresponding probability of value exceeding 12 times of the MAD is $\sim 5.1 \times 10^{-15}$. In reality, some systematic features of waveforms (e.g., converted phases or seismic signals from distant events) may introduce some waveform correlations that look like a detection (e.g., Meng et al., 2013). However, if most of the LFEs are false detections, we would expect to see most of the detections during large-amplitude high-frequency signals. For the 2004 Sumatra and 2005 Nias earthquakes (Figs. 3 and S2), the high-frequency amplitudes of the teleseismic P waves are larger than those during the teleseismic surface waves. However, most LFEs were detected during teleseismic surface waves. Finally, the locations of LFEs during and outside the time window of TTs are similar (Fig. 5), and the background rates long before and after the teleseismic waves are also similar (Fig. 4). Although we cannot exclude all false detections, we consider that most of the LFEs found in this study are genuine detections.

During the surface waves of the 2004 Sumatra earthquake, two local earthquakes with M_L 2.7 and 2.5 took place at depths of 32 and 14 km, respectively, near the region of LFEs epicenters (orange stars in Fig. 1). Whether these two local earthquakes were triggered by the Sumatra mainshock remains to be investigated further. Nevertheless, the occurrence of these two earthquakes did not seem to affect the triggered LFE rates (Fig. 3). A similar case was found in the 2007 Kuril-Island event. An earthquake with M_L 3.0 occurred off the coast of the Eastern Coastal Range, and the corresponding waveform can be seen around ~2100 s (Fig. S3). The apparent quiescence in LFEs followed by a recovery is shown around this event. However, a close look revealed that the quiescence occurred immediately before the P arrival of this event. Hence, it is not clear what caused such variation in the LFEs occurrence. In summary, we found no clear correlations between LFEs and local earthquakes (Figs. 3, S2–S6).

The LFEs were located slightly close to the CLF, and occurred ~10 km deeper than background seismicity (Figs. 1 and 5). Their depth ranges are consistent with the dipping direction of the CLF. However, the LFEs occurred in a restricted volume instead of a linear fault alignment (Figs. 1 and 5). It is possible that that source regions responsible for generating tremors and LFEs are complex and may consist of multiple strands of fault systems with the expected dip of the CLF (Ho, 1988; Tang et al., 2011). The relative location error reported from the hypoDD program is less than 250 m. However, the true errors resulting from inaccurate velocity models and phase picks could be much larger than that, which could also result in a volume-like distribution. Although we used waveform cross-correlations to align P and S waves, the signal-to-noise ratios for individual events are generally low. This could cause cycle skipping or other issues, resulting in inaccurate phase picks and final locations. Another drawback of the current technique is the use of 11 LFE events triggered by the 2005 Nias event as templates to detect new LFEs. Because of this, we can only detect LFEs that are similar to the LFEs triggered by the Nias earthquake. More LFEs can be detected if we use more templates which occurred in slightly different regions, or an auto-correlation approach (Brown et al., 2008). Further studies based on dense array observations (Sun et al., 2011) and improved location techniques could help to better understand the deep fault structures responsible for generating tremor and LFEs in southern Taiwan. Analysis of triggered event data from borehole seismic stations in southern Taiwan may also provide higher quality data for studying LFEs and TTs.

In summary, detecting LFEs from tremors provides not only exciting new understanding about the deep extension of active faults (Shelly et al., 2009; Rubinstein et al., 2010) but also their role in releasing tectonic stresses during large, distant earthquakes (Rubinstein et al., 2007). Furthermore, tremors and LFEs are extremely stress sensitive and hence could potentially act as a natural 'stress meter' to monitor time-dependent changes around deep faults, especially before large earthquakes (Shelly, 2009, 2010). Observations of LFEs and tremors over longer time periods

could potentially contribute to a better understanding of the physical mechanisms and necessary conditions for tremor generation at major plate boundary faults around the world, as well as deep fault zone properties and large earthquake cycles in Taiwan.

Acknowledgments

We thank the Institute of Earth Sciences, Academia Sinica and the Central Weather Bureau for providing the waveform data. This manuscript was benefited from useful comments by Chastity Aiken, the editor Peter Shearer and three anonymous reviewers. This work was supported by the Taiwan Earthquake Research Center (TEC) funded through Taiwan National Science Council (NSC). Zhigang Peng is supported by the US National Science Foundation (EAR-0956051).

Appendix A. Supplementary materials

Supplementary data associated with this article can be found in the online version at http://dx.doi.org/10.1016/j.epsl.2013.04.039.

References

Aiken, C., Peng, Z., Chao, K., 2013. Tremors along the Queen Charlotte Margin triggered by large teleseismic earthquakes. Geophys. Res. Lett. 40, 829–834, http://dx.doi.org/10.1002/GRL.50220.

Aron, A., Hardebeck, J.L., 2009. Seismicity rate changes along the central California coast due to stress changes from the 2003 M 6.5 San Simeon and 2004 M 6.0 Parkfield earthquakes. Bull. Seismol. Soc. Am. 99, 2280–2292, http://dx.doi.org/10.1785/0120080239.

Brodsky, E.E., 2006. Long-range triggered earthquakes that continue after the wave train passes. Geophys. Res. Lett. 33, L15313, http://dx.doi.org/10.1029/2006GL026605.

Brown, J.R., Beroza, G.C., Shelly, D.R., 2008. An autocorrelation method to detect low frequency earthquakes within tremor. Geophys. Res. Lett. 35, L16305, http://dx.doi.org/10.1029/2008GL034560.

Brown, J.R., Beroza, G.C., Ide, S., Ohta, K., Shelly, D.R., Schwartz, S.Y., Rabbel, W., Thorwart, M., Kao, H., 2009. Deep low-frequency earthquakes in tremor localize to the plate interface in multiple subduction zones. Geophys. Res. Lett. 36, L19306, http://dx.doi.org/10.1029/2009GL040027.

Chao, K., Peng, Z., Wu, C., Tang, C.-C., Lin, C.-H., 2012. Remote triggering of non-volcanic tremor around Taiwan. Geophys. J. Int. 188, 301–324, http://dx.doi.org/10.1111/j.1365-246X.2011.05261.x.

Chao, K., Peng, Z., Gonzalez-Huizar, H., Aiken, C., Enescu, B., Kao, H., Velasco, A.A., Obara, K., Matsuzawa, T., 2013. A global search for triggered tremor following the 2011 M_w 9.0 Tohoku Earthquake. Bull. Seismol. Soc. Am. 103, 1551–1571, http://dx.doi.org/10.1785/0120120171.

Fry, B., Chao, K., Bannister, S.C., Peng, Z., Wallace, L., 2011. Deep tremor in New Zealand triggered by the 2010 M_w 8.8 Chile earthquake. Geophys. Res. Lett. 38, L15306, http://dx.doi.org/10.1029/2011GL048319.

Ghosh, A., Vidale, J.E., Peng, Z., Creager, K.C., Houston, H., 2009. Complex nonvolcanic tremor near Parkfield, California, triggered by the great 2004 Sumatra earthquake. J. Geophys. Res. 114, B00A15, http://dx.doi.org/10.1029/2008JB006062.

Gibbons, S.J., Ringdal, F., 2006. The detection of low magnitude seismic events using array-based waveform correlation. Geophys. J. Int. 165, 149–166, http://dx.doi.org/10.1111/j.1365-246X.2006.02865.x.

Gomberg, J., 2010. Lessons from (triggered) tremor. J. Geophys. Res. 115, B01302, http://dx.doi.org/10.1029/2008JB006062.

Gonzalez-Huizar, H., Velasco, A.A., Peng, Z., Castro, R.R., 2012. Remote triggered seismicity caused by the 2011, M9.0 Tohoku-Oki, Japan earthquake. Geophys. Res. Lett. 39, L10302, http://dx.doi.org/10.1029/2012GL051015.

Ho, C.S., 1988. An Introduction to the Geology of Taiwan: Explanatory Text of the Geologic Map of Taiwan. Central Geological Survey, Ministry of Economic Affairs, Taipei, Taiwan.

Katsumata, A., Kamaya, N., 2003. Low-frequency continuous tremor around the Moho discontinuity away from volcanoes in the southwest Japan. Geophys. Res. Lett. 30 (1), 1020, http://dx.doi.org/10.1029/2002GL015981.

Meng, X., Peng, Z., Hardebeck, J., 2013. Seismicity around Parkfield correlates with static shear stress changes following the 2003 M_w 6.5 San Simeon earthquake. J. Geophys. Res., submitted for publication.

Miyazawa, M., Brodsky, E.E., 2008. Deep low-frequency tremor that correlates with passing surface waves. J. Geophys. Res. 113, B01307, http://dx.doi.org/10.1029/2006JB004890.

Miyazawa, M., Brodsky, E.E., Mori, J., 2008. Learning from dynamic triggering of low-frequency tremor in subduction zones. Earth Planets Space 60, e17–e20.

Nadeau, R.M., Dolenc, D., 2005. Nonvolcanic tremors deep beneath the San Andreas Fault. Science 307, 389.

Obara, K., 2002. Nonvolcanic deep tremor associated with subduction in southwest Japan. Science 296, 1679–1681, http://dx.doi.org/10.1126/science.1070378.

Peng, Z., Vidale, J.E., Ishii, M., Helmstetter, A., 2007. Seismicity rate immediately before and after main shock rupture from high-frequency waveforms in Japan. J. Geophys. Res. 112, B03306, http://dx.doi.org/10.1029/2006JB004386.

Peng, Z., Chao, K., 2008. Non-volcanic tremor beneath the Central Range in Taiwan triggered by the 2001 M_w 7.8 Kunlun earthquake. Geophys. J. Int. 175 (2), 825–829.

Peng, Z., Vidale, J.E., Creager, K.C., Rubinstein, J.L., Gomberg, J., Bodin, P., 2008. Strong tremor near Parkfield, CA excited by the 2002 Denali Fault earthquake. Geophys. Res. Lett. 35, L23305, http://dx.doi.org/10.1029/2008GL036080.

Peng, Z., Vidale, J.E., Wech, A., Nadeau, R.M., 2009. Remote triggering of tremor along the San Andreas Fault in central California. J. Geophys. Res. 114, B00A06, http://dx.doi.org/10.1029/2008JB006049.

Peng, Z., Zhao, P., 2009. Migration of early aftershocks following the 2004 Parkfield earthquake. Nat. Geosci. 2, 877–881, http://dx.doi.org/10.1038/NGEO697.

Peng, Z., Hill, D., Shelly, D.R., Aiken, C., 2010. Remotely triggered microearthquakes and tremor in Central California following the 2010 M_w 8.8 Chile Earthquake. Geophys. Res. Lett. 37, L24312, http://dx.doi.org/10.1029/2010GL045462.

Peng, Z., Gomberg, J., 2010. An integrative perspective of coupled seismic and aseismic slow slip phenomena. Nat. Geosci. 3, 599–607, http://dx.doi.org/10.1038/NGEO940.

Peng, Z., Gonzalez-Huizar, H., Chao, K., Aiken, C., Moreno, B., Armstrong, G., 2013. Tectonic tremor in Cuba triggered by large teleseismic earthquakes. Bull. Seismol. Soc. Am. 103 (1), 595–600, http://dx.doi.org/10.1785/0120120253.

Rubinstein, J.L., Vidale, J.E., Gomberg, J., Bodin, P., Creager, K.C., Malone, S.D., 2007. Non-volcanic tremor driven by large transient shear stresses. Nature 448, 579–582.

Rubinstein, J.L., La Rocca, M., Vidale, J.E., Creager, K.C., Wech, A.G., 2008. Tidal modulation of non-volcanic tremor. Science 319, 186–189.

Rubinstein, J.L., Gomberg, J., Vidale, J.E., Wech, A.G., Kao, H., Creager, K.C., Rogers, G., 2009. Seismic wave triggering of non-volcanic tremor, ETS, and earthquakes on Vancouver Island. J. Geophys. Res. 114, B00A01, http://dx.doi.org/10.1029/2008JB005875.

Rubinstein, J.L., Shelly, D.R., Ellsworth, W.L., 2010. Non-volcanic tremor: a window into the roots of fault zones. In: Cloetingh, S., Negendank, Jorg (Eds.), New Frontiers in Integrated Solid Earth Sciences. Springer, Netherlands, New York, pp. 287–314.

Shelly, D.R., Beroza, G.C., Ide, S., Nakamula, S., 2006. Low-frequency earthquake in Shikoku, Japan, and their relationship to episodic tremor and slip. Nature 442, 188–191, http://dx.doi.org/10.1038/nature04931.

Shelly, D.R., Beroza, G.C., Ide, S., 2007. Non-volcanic tremor and low frequency earthquake swarms. Nature 446, 305–307, http://dx.doi.org/10.1038/nature05666.

Shelly, D.R., Ellsworth, W.L., Ryberg, T., Haberland, C., Fuis, G.S., Murphy, J., Nadeau, R.M., Bürgmann, R., 2009. Precise location of San Andreas Fault tremors near Cholame, California using seismometer clusters: slip on the deep extension of the fault? Geophys. Res. Lett. 36, L01303, http://dx.doi.org/10.1029/2008GL036367.

Shelly, D.R., 2009. Possible deep fault slip preceding the 2004 Parkfield earthquake, inferred from detailed observations of tectonic tremor. Geophys. Res. Lett. 36, L17318, http://dx.doi.org/10.1029/2009GL039589.

Shelly, D.R., 2010. Migrating tremors illuminate complex deformation beneath the seismogenic San Andreas fault. Nature 463, 648–652, http://dx.doi.org/10.1038/nature08755.

Shelly, D.R., Hardebeck, J.L., 2010. Precise tremor source locations and amplitude variations along the lower-crustal central San Andreas Fault. Geophys. Res. Lett. 37, L14301, http://dx.doi.org/10.1029/2010GL043672.

Shelly, D.R., Peng, Z., Hill, D.P., Aiken, C., 2011. Triggered creep as a possible mechanism for delayed dynamic triggering of tremor and earthquake. Nat. Geosci. 4, 384–388, http://dx.doi.org/10.1038/NGEO01141.

Sun, W.-F., Lin, C.-H., Peng, Z., Chao, K., 2011. Non-volcanic tremors beneath the Southern Central Range in Taiwan. Abstract S23B-2251 Presented at 2011 Fall Meeting, 5–9 December. AGU. San Francisco, California.

Tang, C.-C., Peng, Z., Chao, K., Chen, C.-H., Lin, C.-H., 2010. Detecting low-frequency earthquakes within non-volcanic tremor in southern Taiwan triggered by the 2005 M_w 8.6 Nias earthquake. Geophys. Res. Lett. 37, L16307, http://dx.doi.org/10.1029/2010GL043918.

Tang, C.-C., Zhu, L., Chen, C.-H., Teng, T.-L., 2011. Significant crustal structural variation across the Chaochou Fault, southern Taiwan: new tectonic implications for convergent plate boundary. J. Asian Earth Sci. 41, 564–570.

Thomas, A.M., Nadeau, R.M., Burgmann, R., 2009. Tremor–tide correlations and near-lithostatic pore pressure on the deep San Andreas fault. Nature 462, 1048–1051, http://dx.doi.org/10.1038/nature08654.

Utsu, T., Ogata, Y., Matsu'ura, R.S., 1995. The centenary of the Omori formula for a decay law of aftershock activity. J. Phys. Earth 43, 1–33.

Velasco, A.A., Hernandez, S., Parsons, T., Pankow, K., 2008. Global ubiquity of dynamic earthquake triggering. Nat. Geosci. 1, 375–379, http://dx.doi.org/10.1038/ngeo204.

Waldhauser, F., Ellsworth, W.L., 2000. A double-difference earthquake location algorithm: method and application to the northern Hayward fault. Bull. Seismol. Soc. Am. 90, 1353–1368.

Wu, Y.-M., Chang, C.-H., Zhao, L., Shyu, J.B.H., Chen, Y.-G., Sieh, K., Avouac, J.-P., 2007. Seismic tomography of Taiwan: improved constraints from a dense network of strong motion stations. J. Geophys. Res. 112, B08312, http://dx.doi.org/10.1029/2007JB004983.

Ziv, A., Rubin, A.M., Kilb, D., 2003. Spatiotemporal analyses of earthquake productivity and size distribution: observations and simulations. Bull. Seismol. Soc. Am. 93, 2069–2081.